

Experimental implementation of arbitrary entangled operations

Seongjin Hong,^{1,2} Chang Hoon Park,^{1,3} Yeon-Ho Choi,^{1,4} Yong-Su Kim,^{1,4} Young-Wook Cho,¹ Kyunghwan Oh,² and Hyang-Tag Lim^{1,*}

¹Center for Quantum Information, Korea Institute of Science and Technology (KIST), Seoul, 02792, Korea

²Institute of Physics and Applied Physics, Yonsei University, Seoul 03722, Korea

³Department of Electrical and Computer Engineering, Ajou University, Suwon 16499, Korea

⁴Division of Nano and Information Technology, KIST School, Korea University of Science and Technology, Seoul 02792, Korea

(Dated: May 7, 2020)

Quantum entanglement lies at the heart of quantum mechanics in both fundamental and practical aspects. The entanglement of quantum states has been studied widely, however, the entanglement of operators has not been studied much in spite of its importance. Here, we propose a scheme to realize arbitrary entangled operations based on a coherent superposition of local operations. Then, we experimentally implement several intriguing two-qubit entangled operations in photonic systems. We also discuss the generalization of our scheme to extend the number of superposed operations and the number of qubits. Due to the simplicity of our scheme, we believe that it can reduce the complexity or required resources of the quantum circuits and provide insights to investigate properties of entangled operations.

Entanglement is the key concept that makes quantum physics distinct from classical physics and plays an essential role in quantum information processing. As an entangled state cannot factor into a product of individual states, entangled operations cannot be represented by a product of individual operations but a coherent superposition of operations [1–5]. To date, superpositions of operators have been studied in both fundamental and practical aspects. Commutation relations for bosonic operators [6] and Pauli operators [7, 8] have been directly demonstrated experimentally using superpositions of operators. Recently, it is reported that the superpositions of quantum operations can allow controlling the orders of quantum operations, which is not allowed in the traditional formalism of quantum physics [9–11]. This, so-called *superposition of causal orders*, is not only fundamentally interesting but also proven that it has practical applications in quantum information processing in the context of communication complexity [12, 13], witnessing causality [14, 15], quantum metrology [16], and transmission of quantum information [17].

However, so far research on superposition of quantum operations has been limited to superposition of single qubit gates in most cases, meaning that entanglement of operators has not been studied much yet. Most of the implementations of superposition of causal orders are relying on the interferometric scheme, however, in this case extension to an entangled operation is not straightforward since nonlocality should be involved. Extension to implementing an entangled operation is particularly important since a two-qubit entangled operation such as controlled-NOT (CNOT) gate can constitute the universal sets of quantum gates with single qubit

gates [18–20]. Implementation of entangled operations for two-qubit systems can provide further advantages for practical quantum information processing, such as entanglement filter [21–23], entangling gate for universal quantum gate set [24], and entanglement generation for teleportation-based programmable quantum gate [7, 25–27]. It is also intriguing to explore entangled operations in even larger Hilbert spaces for investigating potential applications in quantum information processing.

In this letter, we propose and demonstrate a scheme for realizing an arbitrary entangled operation based on a coherent superposition of local operations. We first begin by introducing the concept of operator entanglement using an operator-Schmidt decomposition. We then present some intriguing and important operations that can be realized based on this scheme in two-qubit systems. Then, we describe our experimental demonstration of several two-qubit entangled operations in photonic systems and discuss our experimental results. Finally, we extend our scheme to the case of generalized entangled operations with N qubit systems and the Schmidt number M . We also present a practical scheme on implementing three-qubit entangled operations and introduce interesting three-qubit operations that can be implemented.

An operator \mathcal{O}_{AB} acting on systems A and B can be written as

$$\mathcal{O}_{AB} = \sum_i c_i \mathcal{O}_A^i \otimes \mathcal{O}_B^i, \quad (1)$$

where $c_i \geq 0$ and \mathcal{O}_A^i (\mathcal{O}_B^i) is orthonormal bases for a system A (B) [5]. Similar to the Schmidt representation of quantum states, Equation (1) is the operator-Schmidt decomposition and the number of nonzero Schmidt coefficients c_i is defined as a Schmidt number [5]. If the Schmidt number of an operator \mathcal{O}_{AB} is larger than one, \mathcal{O}_{AB} is an entangled operator meaning that it can gen-

* hyangtag.lim@kist.re.kr

erate entanglement from separable states. It is clear from Eq. (1) that an entangled operation cannot be prepared by local operations and classical communications (LOCC) between two distant systems A and B. In general, an operator having higher Schmidt number needs more resources to be constructed [5].

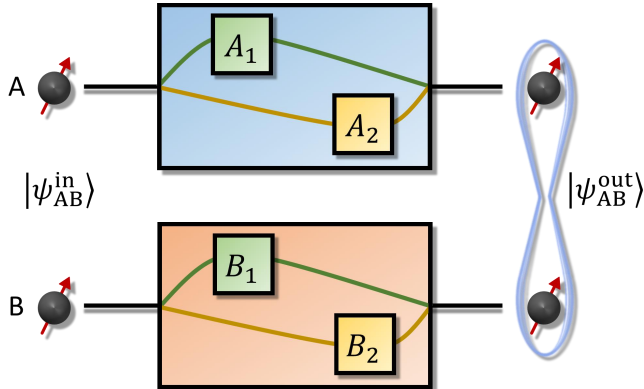


FIG. 1. Concept of two-qubit entangled operation with the Schmidt number 2. Two-qubit input states $|\psi_{AB}^{\text{in}}\rangle$ undergoes either operation $A_1 \otimes B_1$ (green line) or $A_2 \otimes B_2$ (orange line). Here, these two processes are coherently superposed so that the output state is $|\psi_{AB}^{\text{out}}\rangle = \frac{1}{\sqrt{2}}(A_1 \otimes B_1 + e^{i\phi} A_2 \otimes B_2) |\psi_{AB}^{\text{in}}\rangle$. For a separable input state, the output state can be entangled. Note that the entangled operation can be implemented only with local operations if we use additional degree of freedom (ancillary systems).

Let us consider a simple case with the Schmidt number 2 and $c_1 = c_2$. Then,

$$\begin{aligned} \mathcal{O}_{AB} &= \frac{1}{\sqrt{2}} (\mathcal{O}_A^1 \otimes \mathcal{O}_B^1 + \mathcal{O}_A^2 \otimes \mathcal{O}_B^2) \\ &= \frac{1}{\sqrt{2}} (A_1 \otimes B_1 + e^{i\phi} A_2 \otimes B_2), \end{aligned} \quad (2)$$

where $\mathcal{O}_A^1 = A_1$, $\mathcal{O}_A^2 = A_2$, $\mathcal{O}_B^1 = B_1$, $\mathcal{O}_B^2 = e^{i\phi} B_2$ and ϕ is the relative phase between $A_1 \otimes B_1$ and $A_2 \otimes B_2$. Note that the second line of Eq. (2) is not the Schmidt decomposition due to the complex number of coefficients, but it can explicitly show the relative phase ϕ between two superposed operations. In many cases, local operations are fixed but their relative phase can be varied. The entangled operation of Equation (2) has a simple form, however, there are intriguing operations. When $A_1 = B_1 = I$, $A_2 = B_2 = \sigma_x$, Equation (2) becomes

$$\frac{1}{\sqrt{2}} (I \otimes I + e^{i\phi} \sigma_x \otimes \sigma_x) = \frac{1}{\sqrt{2}} \begin{pmatrix} 1 & 0 & 0 & e^{i\phi} \\ 0 & 1 & e^{i\phi} & 0 \\ 0 & e^{i\phi} & 1 & 0 \\ e^{i\phi} & 0 & 0 & 1 \end{pmatrix}, \quad (3)$$

where I is an identity operation and σ_x , σ_y , and σ_z are Pauli operators. One can prepare maximally entangled states $\frac{1}{\sqrt{2}}(|00\rangle + e^{i\phi}|11\rangle)$ ($\frac{1}{\sqrt{2}}(|01\rangle + e^{i\phi}|10\rangle)$) from a separable input state $|00\rangle$ ($|01\rangle$).

When $A_1 = |0\rangle\langle 0|$, $B_1 = I$, $A_2 = |1\rangle\langle 1|$, and $B_2 = U$ where U is a single qubit unitary operation, one can implement a controlled-Unitary (CU) operation. In addition, by setting $A_1 = B_1 = |0\rangle\langle 0|$, $A_2 = B_2 = |1\rangle\langle 1|$, one can realize the entanglement filter (EF) which is a special non-unitary operation, and transmits the input states only when the incoming qubit states is either $|0\rangle|0\rangle$ or $|1\rangle|1\rangle$ [21–23].

However, it is difficult to implement an entangled operation of Equation (2). Using an interferometer, it is possible to make a superposition of two different operators such as $\mathcal{O}_A = 1/\sqrt{2}(A_1 + e^{i\phi} A_2)$ [8]. However, when the system A and B use interferometers separately, what they prepare is $1/2(A_1 + e^{i\phi} A_2) \otimes (B_1 + e^{i\phi} B_2)$, which has clearly the Schmidt number 1. Note that if we apply A_1 and B_1 simultaneously to the system A and B with the half of the time and apply A_2 and B_2 with another half of the time, the prepared operation is an incoherent mixture of $A_1 \otimes B_1$ and $A_2 \otimes B_2$ rather than a coherent superposition of them.

Here, we propose a scheme for implementing an entangled operations using additional degree of freedom. The conceptual diagram of our scheme is shown in Fig. 1. For a two-qubit input state $|\psi_{AB}^{\text{in}}\rangle$, qubit A undergoes an operation A_1 or A_2 while qubit B undergoes an operation B_1 or B_2 . In order to prepare an entangled operation, one needs to rule out $A_1 \otimes B_2$ and $A_2 \otimes B_1$ cases and the other two cases $A_1 \otimes B_1$ and $A_2 \otimes B_2$ should be coherently superposed. It is difficult to achieve these requirements, however, it is possible by using energy-time correlation of spontaneous parametric down conversion (SPDC) process. In experiment, the input state is encoded in a polarization of single photons. When a pair of photons are generated via SPDC process, the generated photon pairs have strong energy-time correlation. By exploiting this strong time correlation between two photons, one can prepare a coherent superposition of local operations, e.g., $\frac{1}{\sqrt{2}}(A_1 \otimes B_1 + e^{i\phi} A_2 \otimes B_2)$ acting on polarization states of two-photons.

The schematic of our experimental setup is shown in Fig. 2, which is based on Franson interferometer [28, 29]. We use a femtosecond pulsed laser operating at a center wavelength of 780 nm and a pulse period of 12.5 ns. The wavelength of the pump laser becomes 390 nm using a lithium triborate (LBO) crystal via second harmonic generation process. Then, a pair of photons is generated via type-II SPDC process by pumping a 1 mm-thick BBO crystal, and its polarization state is prepared in an arbitrary input state $|\psi_{AB}^{\text{in}}\rangle$ with a set of polarizer, half and quarter wave plates (WPs). Then, each photon is sent to an unbalanced Michelson interferometer (UMI) with different optical lengths of L_1 and L_2 . The path length different $L = L_2 - L_1$ is 1.875 m corresponding to an half of the pulse period of the pump laser to ensure that the down-converted photons generated from consecutive pump pulses are temporally overlapped. Here we

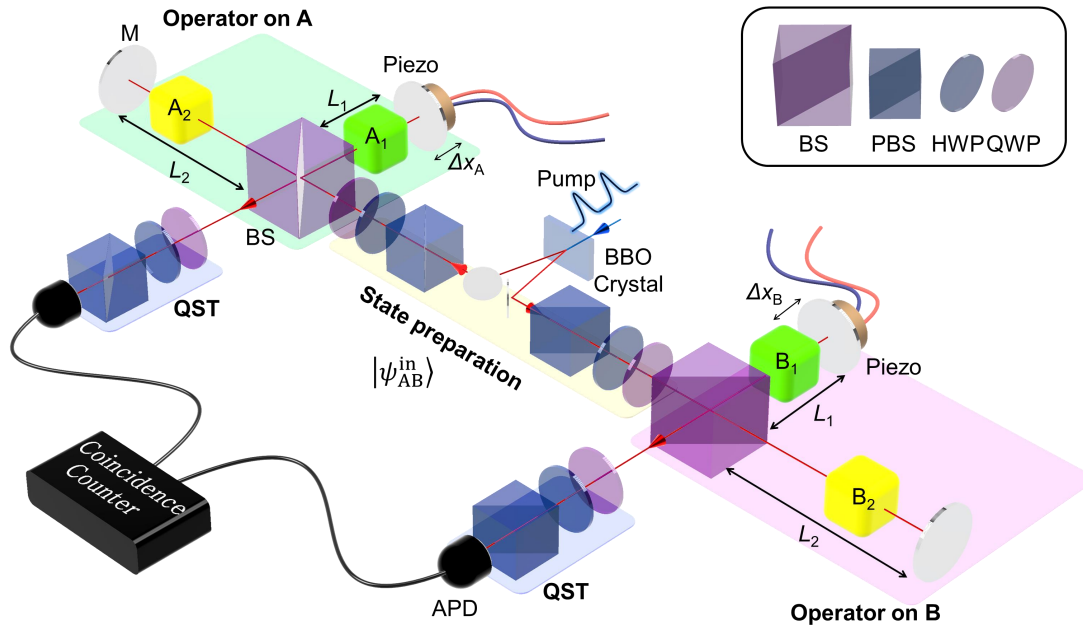


FIG. 2. Schematic of the experimental set-up. A down-converted photon pair generated from a pulsed laser is prepared in an arbitrary polarization two-photon state $|\psi_{AB}^{\text{in}}\rangle$ using a set of Pol., HWP, and QWP. Single qubit operations (A_1 , A_2 , B_1 , and B_2) can be realized with linear optical elements such as Pol. and WPs, and the relative phase between two arms of an unbalanced Michelson interferometer (UMI) is controlled by adjusting Δx_A and Δx_B , respectively. Entangled operations are implemented with two UMIs. A set of Pol. and WPs in front of APD are used to perform QST measurements (BBO: Beta Barium borate crystal, QST: Quantum state tomography, M: Mirror, APD: Avalanche photo diode, QWP: Quarter waveplate, HWP: Half waveplate, Pol.: Polarizer, BS: Beam splitter, PBS: Polarizing beam splitter).

use an interference filter with 2 nm full-width at half maximum bandwidth, then the coherence length of each down-converted photon is around $300 \mu\text{m}$. Hence, there is no first order interference at the output of UMI. In order to implement \mathcal{O}_{AB} in Equation (2), single qubit operations A_1 and A_2 (B_1 and B_2) are located in L_1 and L_2 arms of the UMI for a photon A (photon B), respectively. Note that a single qubit operation can be realized by linear optical elements such as WPs, polarizers, and so on. The two-photon output states are analyzed by a set of WPs and polarizers using quantum state tomography (QST) and quantum process tomography (QPT).

There are four possible output cases for the two-photon input states: $A_1 \otimes B_1 |\psi_{AB}^{\text{in}}\rangle$, $A_1 \otimes B_2 |\psi_{AB}^{\text{in}}\rangle$, $A_2 \otimes B_1 |\psi_{AB}^{\text{in}}\rangle$, and $A_2 \otimes B_2 |\psi_{AB}^{\text{in}}\rangle$. However, if we set the coincidence window (we use 3 ns) smaller than the time difference between L_1 and L_2 (12.5 ns), we can post-select only $A_1 \otimes B_1 |\psi_{AB}^{\text{in}}\rangle$ and $A_2 \otimes B_2 |\psi_{AB}^{\text{in}}\rangle$ events. Note that this is possible due to strong time correlation between generated photon pairs. Therefore, the post-selected output state $|\psi_{AB}^{\text{out}}\rangle$ becomes $\frac{1}{\sqrt{2}} (A_1 \otimes B_1 + e^{i\phi} A_2 \otimes B_2) |\psi_{AB}^{\text{in}}\rangle$ where ϕ is the sum of relative phase differences in each UMI ($\phi = \phi_A + \phi_B$). In order to fix ϕ , we attached piezoelectric actuators on both mirrors in the short arms of the UMI and drive them using proportional integral derivative (PID) controllers to

lock the relative phases ϕ_A and ϕ_B . Here, we can choose ϕ between 0 to 2π using a set of QWP, HWP, and QWP on the locking laser (780 nm pump laser). See Appendix for detailed information on the controllable phase-locking technique we use.

We demonstrated various entangled operations based on our experimental setup shown in Fig. 2. The first entangled operation we consider is $\mathcal{O}_{AB}(\phi)$ with $A_1 = B_1 = \sigma_z$ and $A_2 = B_2 = \sigma_x$, i.e., $\mathcal{O}_{AB}(\phi) = \frac{1}{\sqrt{2}} (\sigma_z \otimes \sigma_z + e^{i\phi} \sigma_x \otimes \sigma_x)$. $\mathcal{O}_{AB}(\phi)$ is able to generate entanglement since for a separable input state $|HH\rangle$, the output state is $|\psi_{AB}^{\text{out}}\rangle = \frac{1}{\sqrt{2}} (|HH\rangle + e^{i\phi}|VV\rangle)$, the maximally entangled states. We implemented $\mathcal{O}_{AB}(\phi)$ with $\phi = 0, \pi/2, \pi$, and $3\pi/2$ and performed quantum state tomography (QST) measurement to each output states. The density matrices of the output states are reconstructed using maximum-likelihood method [30, 31] and the experimental results are shown in Fig. 3. As shown in Fig. 3, one can adjust the relative phase ϕ and the realized operation works well. Note that for the input state $|HV\rangle$, the output state becomes $|\psi_{AB}^{\text{out}}\rangle = \frac{1}{\sqrt{2}} (|HV\rangle - e^{i\phi}|VH\rangle)$. See Appendix for experimental results for the input state $|HV\rangle$.

In order to show the quality of the implemented operation, we also performed quantum process tomography (QPT) measurement. Figure 4 shows the experimentally

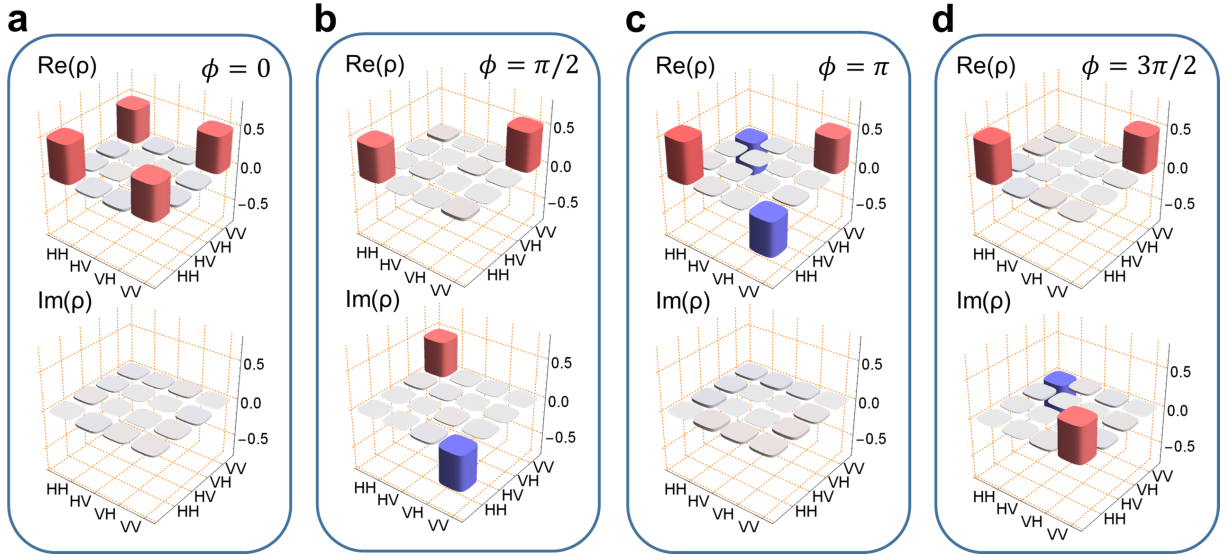


FIG. 3. Reconstructed density matrices of the output state after the entangled operation $\mathcal{O}_{AB} = \frac{1}{\sqrt{2}} (\sigma_z \otimes \sigma_z + e^{i\phi} \sigma_x \otimes \sigma_x)$. Input state is prepared to $|HH\rangle$, and σ_x and σ_z are implemented by using QWP with an angle of $\pi/4$ and 0, respectively. The expected output state after the entangled operation is $\frac{1}{\sqrt{2}} (|HH\rangle + e^{i\phi}|VV\rangle)$. The reconstructed density matrices of the output states correspond to (a) $\phi = 0$, (b) $\pi/2$, (c) π , and (d) $3\pi/2$. Note that the upper (lower) rows corresponds to the real (imaginary) part of the density matrices. The average fidelity between the ideal output state and the experimentally obtained output state is $F_{\text{ave}} = 0.940 \pm 0.014$ and the average concurrence of the output states $C = 0.906 \pm 0.025$. We performed Monte-Carlo simulations on reconstructing density matrices of each output state 100 times and the calculated experimental errors corresponds to one standard deviation.

reconstructed process matrices χ for entangled operations $\frac{1}{\sqrt{2}} (\sigma_z \otimes \sigma_z + \sigma_x \otimes \sigma_x)$ and $\frac{1}{\sqrt{2}} (I \otimes I + i\sigma_x \otimes \sigma_x)$. The corresponding process fidelities F_χ are 0.760 ± 0.005 and 0.762 ± 0.006 , respectively. Here we use $F_\chi = \left[\text{Tr}(\sqrt{\chi_{\text{exp}} \chi_{\text{ideal}} \chi_{\text{exp}}}) \right]^2$ where χ_{ideal} (χ_{exp}) is the process matrix of the ideal (experimentally realized) operation. Note that F_χ results are obtained by performing 100 Monte-Carlo simulations on the QPT measurement results and the errors on the process fidelities corresponds to one standard deviation. We also provide QPT results of $\frac{1}{\sqrt{2}} (I \otimes I - \sigma_x \otimes \sigma_x)$ operation in Appendix. We attribute the non-unity process fidelity to the imperfections of our experimental setup. We provide performance test results of our phase stability setup in Supplementary Note. We emphasize that non-unity process fidelity is not due to the limitation of our proposed scheme but the imperfection of our experimental demonstration.

Note that in general, a coherent superposition of unitary operators is not a unitary operator. The operator $\frac{1}{\sqrt{2}} (\sigma_z \otimes \sigma_z + \sigma_x \otimes \sigma_x)$ is composed of unitary operators but it is a non-unitary operator. On the other hand, $\frac{1}{\sqrt{2}} (I \otimes I + i\sigma_x \otimes \sigma_x)$ is a unitary operation. It is known that if U_{AB} is a two-qubit unitary operation with Schmidt number 2, U_{AB} has the form of $\sqrt{1-p} I \otimes I + i\sqrt{p} \sigma_x \otimes \sigma_x$ up to local unitary equivalence where $0 \leq p \leq 1$ [5]. Hence, one can realize any two-qubit unitary operations with Schmidt number 2 using our scheme. Moreover,

it is interesting to consider the possibility of emulating Ising gate, which is a two-qubit gate implemented natively in trapped-ion quantum system, based on our scheme [32, 33]. For example, $\frac{1}{\sqrt{2}} (I \otimes I + i\sigma_x \otimes \sigma_x)$ is exactly the same with $3\pi/4$ Ising (XX) gate [33]. Note that, Ising (XX) gate and single-qubit rotation gates can constitute a universal set of quantum gates.

We emphasize that entangled operations can be extended to the case of M superposed operations \mathcal{O}_N^M for N qubit states by adding optical arms of the interferometers and adding the number of interferometers, respectively, then \mathcal{O}_N^M is given by

$$\mathcal{O}_N^M = \sum_{k=1}^M c_k \mathcal{O}_k^{(1)} \otimes \dots \otimes \mathcal{O}_k^{(N)}, \quad (4)$$

where $\mathcal{O}_k^{(j)}$ is the k -th local operation acting on j -th qubit and c_k is the Schmidt coefficient. Figure 5(a) shows an unbalanced Mach-Zehnder interferometer (UMZI) with four different arms. For an interferometer A, the local operation A_i with $i = 0, 1, 2, 3$ is located in each arm of the UMZI where the optical path length difference is fixed to L between two neighboring arms and it is the same for the interferometer B. Then, one can prepare an entangled operation with Schmit number 4 of

$$\frac{1}{2} (A_1 \otimes B_1 + e^{i\phi_1} A_2 \otimes B_2 + e^{i\phi_2} A_3 \otimes B_3 + e^{i\phi_3} A_4 \otimes B_4), \quad (5)$$

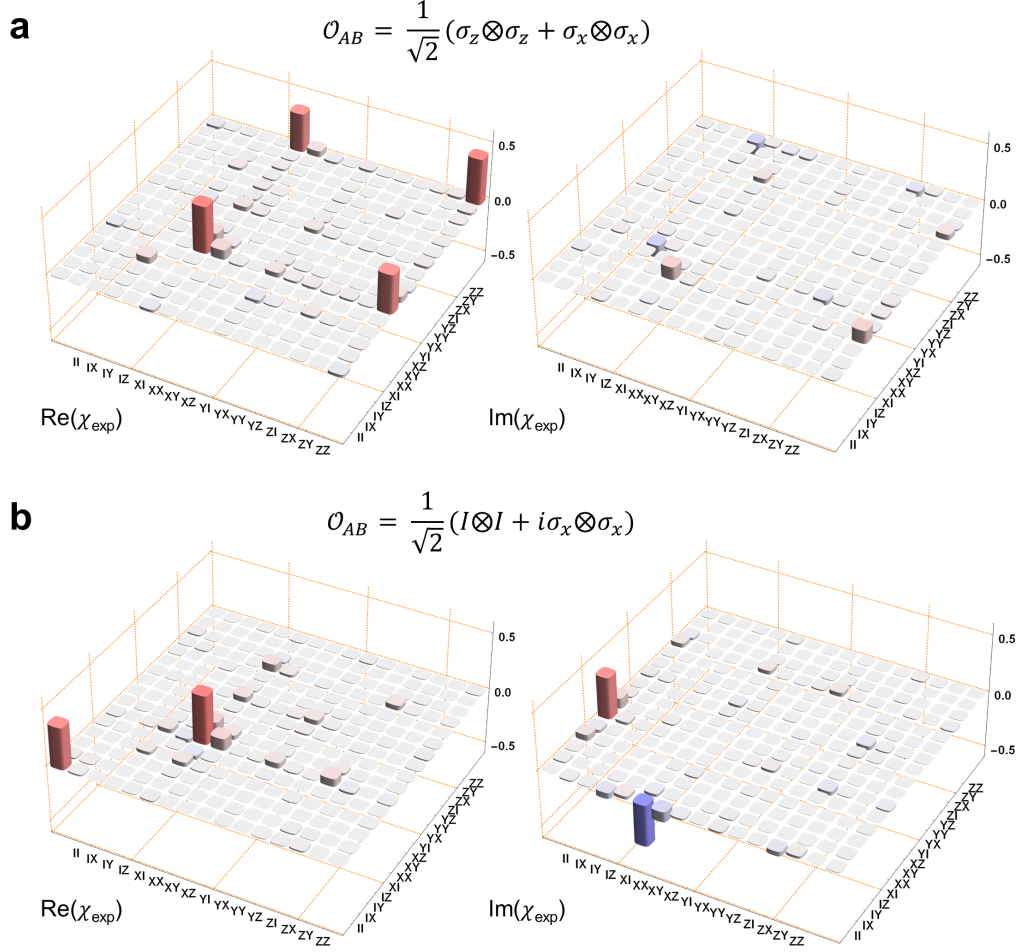


FIG. 4. Experimentally reconstructed process matrices χ of the entangled operations. (a). $\mathcal{O}_{AB} = \frac{1}{\sqrt{2}} (\sigma_z \otimes \sigma_z + \sigma_x \otimes \sigma_x)$. (b) $\mathcal{O}_{AB} = \frac{1}{\sqrt{2}} (I \otimes I + i\sigma_x \otimes \sigma_x)$. We reconstructed process matrices using maximum-likelihood method on quantum process tomography results. Left (right) columns corresponds to the real (imaginary) part of the process matrices. Process matrices are represented in the Pauli basis, for example, YZ corresponds to σ_y, σ_z basis.

by post-selecting the case where the arrival time difference of two-photons is zero and ϕ_i with $i = 1, 2, 3$ is the relative phase differences. In this case, all the other terms are not detected [28, 29]. It is well-known that any two-qubit operation can be decomposed into the form of Eq. (5) up to local unitary equivalence [34]. Note that we can implement SWAP gate $\frac{1}{2} (I \otimes I + \sigma_x \otimes \sigma_x + \sigma_y \otimes \sigma_y + \sigma_z \otimes \sigma_z)$ based on the setup shown in Fig. 5(a). Considering the CNOT complexity of SWAP gate is three [35], i.e., three consecutive CNOT gates are required for a single SWAP gate, it significantly reduces the implementation complexity of SWAP gate.

We can also consider increasing the number of qubits by adding more UMZIs as shown in Fig. 5(b). For example, three photon input states can be prepared by using cascaded SPDC process [36]. In this case, we consider three qubit systems and the corresponding three qubit

entangled operation \mathcal{O}_3^M is

$$\mathcal{O}_3^M = \sum_{k=1}^M c_k \mathcal{O}_k^A \otimes \mathcal{O}_k^B \otimes \mathcal{O}_k^C, \quad (6)$$

where \mathcal{O}_k^C are single qubit operations acting on qubit C. For example, one can obtain three qubit Greenberger-Horne-Zeilinger (GHZ) state [37] $|GHZ\rangle = \frac{1}{\sqrt{2}} (|HHH\rangle + |VVV\rangle)$ from an input state $|HHH\rangle$ by implementing $\frac{1}{\sqrt{2}} (I \otimes I \otimes I + \sigma_x \otimes \sigma_x \otimes \sigma_x)$. Likewise, if one implement $\frac{1}{\sqrt{3}} (I \otimes I \otimes \sigma_x + I \otimes \sigma_x \otimes I + \sigma_x \otimes I \otimes I)$, then one can prepare three qubit W state [38] $|W\rangle = \frac{1}{\sqrt{3}} (|HHV\rangle + |HVH\rangle + |VHH\rangle)$ from an input state $|HHH\rangle$. Moreover, one can implement the controlled-controlled-unitary (CCU) gate $\mathcal{O}_{CCU} = |H\rangle\langle H| \otimes |H\rangle\langle H| \otimes I + |H\rangle\langle H| \otimes |V\rangle\langle V| \otimes I + |V\rangle\langle V| \otimes |H\rangle\langle H| \otimes I + |V\rangle\langle V| \otimes |V\rangle\langle V| \otimes U$.

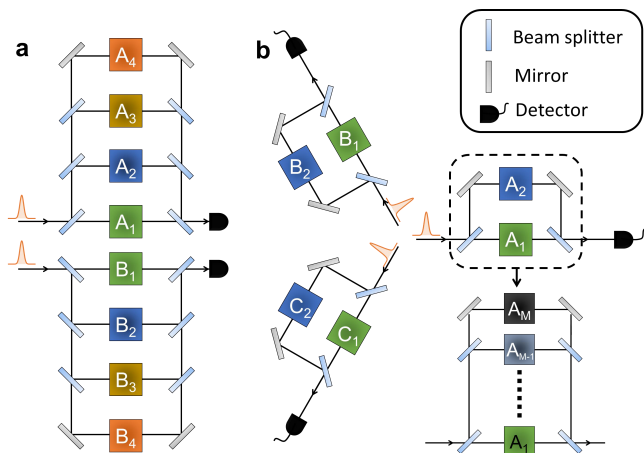


FIG. 5. Generalization to the entangled operation with higher Schmidt number and multipartite systems. (a) For two-qubit input states, one can increase the number of optical paths of the UMZI. Then, the entangled operation with higher Schmidt number can be realized. (b) By adding one more UMZI, one can implement tripartite entangled operations.

If $U = \sigma_x$, then this operation becomes the Toffoli (controlled-controlled NOT) gate [39]. So far, we only consider superposition of local operations with equal amplitudes but the amplitude of each operation can be varied by adjusting transmittance and reflectance of beam splitters.

In summary, we have proposed a scheme to implement arbitrary entangled operations based on a coherent superposition of local operations. We also report an experimental demonstration of various two-qubit entangled operations in photonic systems. We believe that our scheme has great importance both in fundamental and practical aspects. Entanglement of operators is closely related to the evolution of quantum systems under non-local Hamiltonians and the entangling power of quantum operators [2, 3, 40]. In addition, it is known that superposition of quantum gates cannot be represented by the conventional quantum circuit models [41] and the extended quantum circuit model allowing such superposition of operators can reduce the computational complexity of some problems and simplify realization of various quantum information processing [10, 42]. Due to the simplicity of our scheme and the possibility to extend to multi-qubit systems, it is interesting to apply our scheme to solve practical problems using quantum algorithms such as quantum chemistry problem [43]. Moreover, although we mainly discuss unitary operations but the scheme can also be applicable to non-trace-preserving operations. Hence, it is intriguing to consider exploring PT symmetry broken operations [44] and adding a control to weak measurements or partial collapse measurement [45].

APPENDIX

Experimental details

390 nm pulse train is prepared by 1 mm thick Lithium triborate (LBO) crystal via second-harmonic generation (SHG) process using a 780 nm mode-locked pump laser (80 MHz repetition rate, 140 fs pulse duration, $M^2 < 1.1$, Chameleon, Coherent), and generates photon pairs via type-II spontaneous parametric down-conversion (SPDC) process at a 1 mm thick beta-barium borate (BBO) crystal. The 780 nm pump laser is separated by a dichroic mirror (DM) from 390 nm laser, and used as a locking laser to lock the relative phase between two arms of an unbalanced Michelson interferometer (UMI). The locking laser enters a one-inch cube beam splitter (BS) spatially separated from the single photon's path in order not to be detected at APD. In order to actively lock the relative phase between two arms of UMI from mechanical and thermal vibrations of optical components, we implement a proportional-integral-derivative (PID) control system as shown in Fig. 6.

Locking the relative phase between two arms of an unbalanced Michelson interferometer

We test the performance of our phase locking system using a single balanced Michelson interferometer (MI), meaning that the path length difference between two arms is negligible. Single photon and locking laser are injected to a single balance MI, and the intensity of the locking laser is controlled by driving the voltage to a piezo actuator attached on the mirror of one arm. Then, we measure the single photon count of the signal (down-converted photons) using an APD depending on the intensity of the locking laser. As shown in Fig. 7(a), we can observe the interference fringes of both signal (black line) and locking laser (red line) at the same time by scanning the mirror on one arm using a piezo actuator (See Fig. 7(a) after 3600 s). Then, we fixed the intensity of the locking laser around the half of the maximum intensity of the interference fringe by using a PID controller and a voltage amplifier, which enables locking the relative phase between two arms of MI. As shown in Fig. 7(a), signal is locked to have the minimum count by adjusting the phase using α when intensity of the locking laser is half of the maximum intensity of interference fringe. Figure 7(b) shows the stability of phase locking in the interferometer during an hour, we find that the relative phase on signal is locked. We have considered that the imperfections of our experimental results (purity, concurrence, and fidelity) are mainly due to the phase fluctuation. We implement an entangled operation $\frac{1}{\sqrt{2}}(A_1 \otimes B_1 + e^{i\phi} A_2 \otimes B_2)$ using a single UMI instead of two UMIs and the results shows the better performance. We will compare this re-

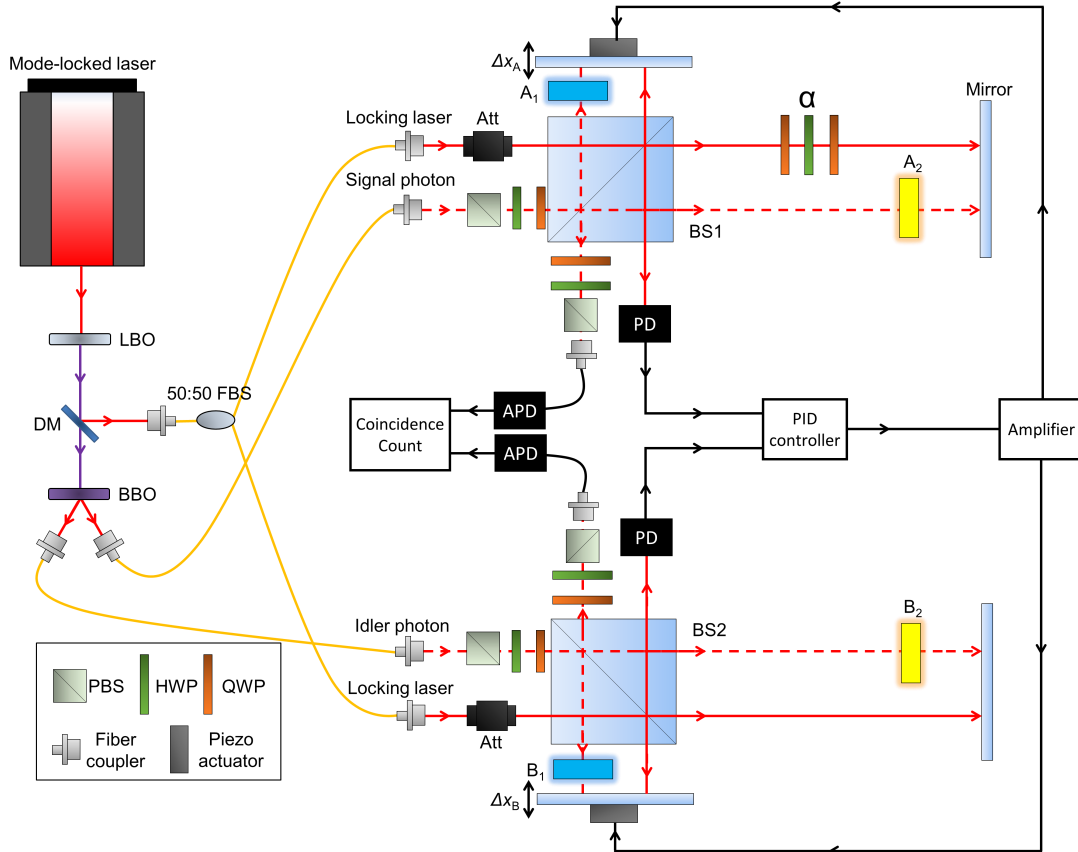


FIG. 6. Experimental setup for implementing two-qubit entangled operation $\frac{1}{\sqrt{2}} (A_1 \otimes B_1 + e^{i\phi} A_2 \otimes B_2)$. LBO: Lithium triborate, DM: dichroic mirror, FBS: fiber beam splitter, BBO: beta-barium borate, BS: beam splitter, PBS: polarizing beam splitter, HWP: half wave plate, QWP: quarter wave plate, PID: proportional-integral-derivative, PD: photo detector, APD: avalanche photo diode, Att: attenuator.

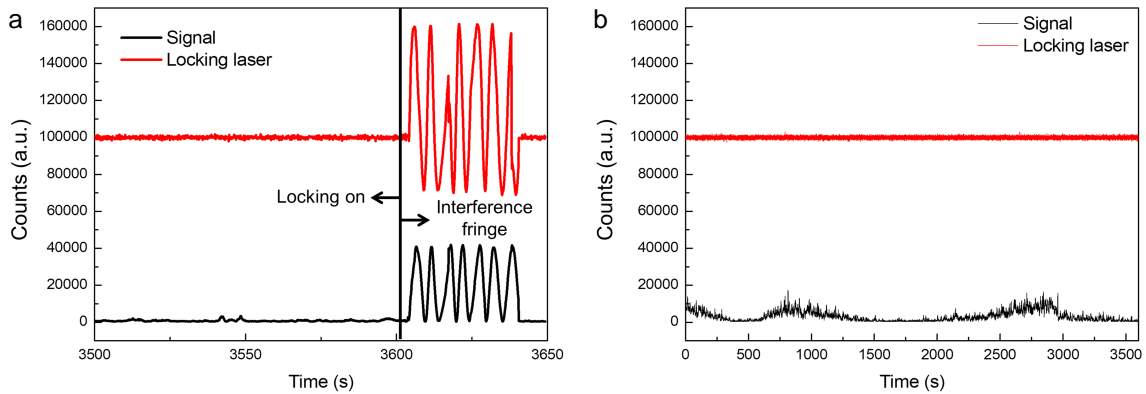


FIG. 7. Results on active phase locking of an Michelson interferometer. The relative phase of an balanced MI is locked by fixing the intensity of locking laser to around the half of the maximum intensity, and we find that single photon signal is also locked simultaneously. Red (black) line corresponds to the intensity of the locking laser (single photon signals). (a) Correlation between the locking laser intensity and the single photon signal. They are locked at the same time during phase locking is on. We can observe that interference fringes of the locking laser and the signal simultaneously by applying a periodic voltage to the piezo actuator. (b) We monitor the intensity change of the locking laser and the signal during an hour while the locking system is on.

sults at the Section III.

In order to control the relative phase ϕ of $\frac{1}{\sqrt{2}}(A_1 \otimes B_1 + e^{i\phi} A_2 \otimes B_2)$ from 0 to 2π in two UMIs, we use a set of QWP($\pi/4$)-HWP(α)-QWP($\pi/4$) for locking laser on the long arm of the UMI on qubit A, see Fig. 6. This waveplate combination provides the phase retardation $\phi = 4\alpha + \pi$ [46] depending on the HWP's angle α while the polarization is unchanged. Note that, this set of WPs gives a phase shift only for locking laser (not signal). If we give phase difference between two arms of UMI by changing the HWP's angle α , the intensity will be changed according to phase difference from α . However, the optical path length difference is shifted depending on α while keeping the intensity of locking laser at half maximum of the interference fringe using PID control, and it enables a relative phase to be adjustable to any value from 0 to 2π .

Experimental setup with a single UMI instead of two

In order to confirm that imperfections of our experimental results are mainly from our phase locking system on the UMIs, we realize the same experiment using a single UMI [47, 48] rather than two UMIs as shown in Fig. 8. Here we send the signal and idler photons into a single BS with a locking laser. Then we can lock the phase of a single UMI instead of two using a single locking laser beam. In this setup, we carry out quantum state tomography of the output state for the entangled operation $\frac{1}{\sqrt{2}}(\sigma_z \otimes \sigma_z + e^{i\phi} \sigma_x \otimes \sigma_x)$ and the results for the input state $|HH\rangle$ is shown in Fig. 9. We compare the experimental results for two cases: a single UMI and two UMI setups in Table I. By decreasing the number of phase locking from two to one, the experimental results are improved. Purity, fidelity, and concurrence of the output state increase about 0.038, 0.027, and 0.039, respectively. Nevertheless, we have to use two UMI setup of Fig. 6 due to the limited spaces for mounting various waveplates required to perform quantum state tomography (QST) and quantum process tomography (QPT). However the comparison summarized in Table I suggests that reducing number of interferometer can increase the quality of the realized operation. Thus, we believe that our phase locking system have room for improvement.

	1 UMI	2 UMIs
Purity	0.942 ± 0.018	0.904 ± 0.025
Fidelity	0.967 ± 0.010	0.940 ± 0.015
Concurrence	0.945 ± 0.017	0.906 ± 0.025

TABLE I. Comparison of experimental results obtained with the setups consisting of either single or double UMIs.

Additional data of QST and QPT

In this section, we provide additional experimental data that are not included in the main text. At first, Fig. 10 shows the reconstructed output states after applying $1/\sqrt{2}(\sigma_z \otimes \sigma_z + e^{i\phi} \sigma_x \otimes \sigma_x)$ entangled operation and the expected output state is $1/\sqrt{2}(|HV\rangle + e^{i\phi}|VH\rangle)$ for the input state $|HV\rangle$. See Figure 3 of the main text for comparison.

Furthermore, we perform quantum process tomography measurement on $\frac{1}{\sqrt{2}}(I \otimes I - \sigma_x \otimes \sigma_x)$ entangled operation and the experimentally reconstructed process matrix χ_{exp} is shown in Supplementary Figure 11. The process fidelity of χ_{exp} with respect to the ideal operation is 0.830 ± 0.008 , which is obtained by performing Monte-Carlo simulations 100 times on the experimental data and the error corresponds to one standard deviation.

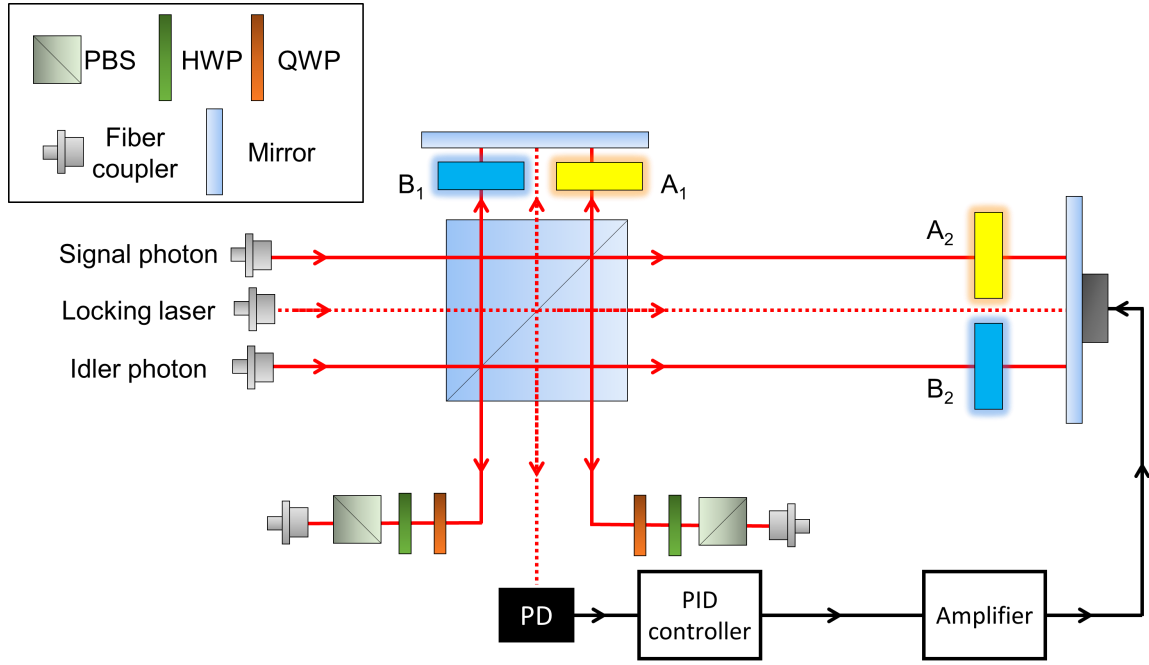


FIG. 8. Experimental setup for implementing $\frac{1}{\sqrt{2}} (A_1 \otimes B_1 + e^{i\phi} A_2 \otimes B_2)$ entangled operation using a single UMI. This corresponds to the simplified version of the setup shown in Fig. 6. Note that the number of UMI is reduced from two to one, meaning that phase locking is required for only one interferometer.

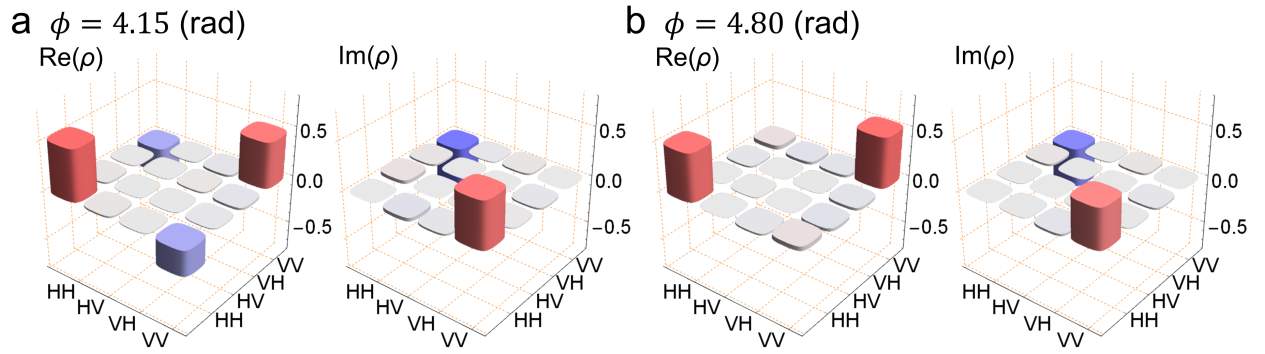


FIG. 9. Experimental QST results with single UMI setup shown in Fig. 8. The realized entangled operation is $\frac{1}{\sqrt{2}} (\sigma_z \otimes \sigma_z + e^{i\phi} \sigma_x \otimes \sigma_x)$ and the input state is $|HH\rangle$. (a) $\phi = 4.15$ and (b) $\phi = 4.80$.

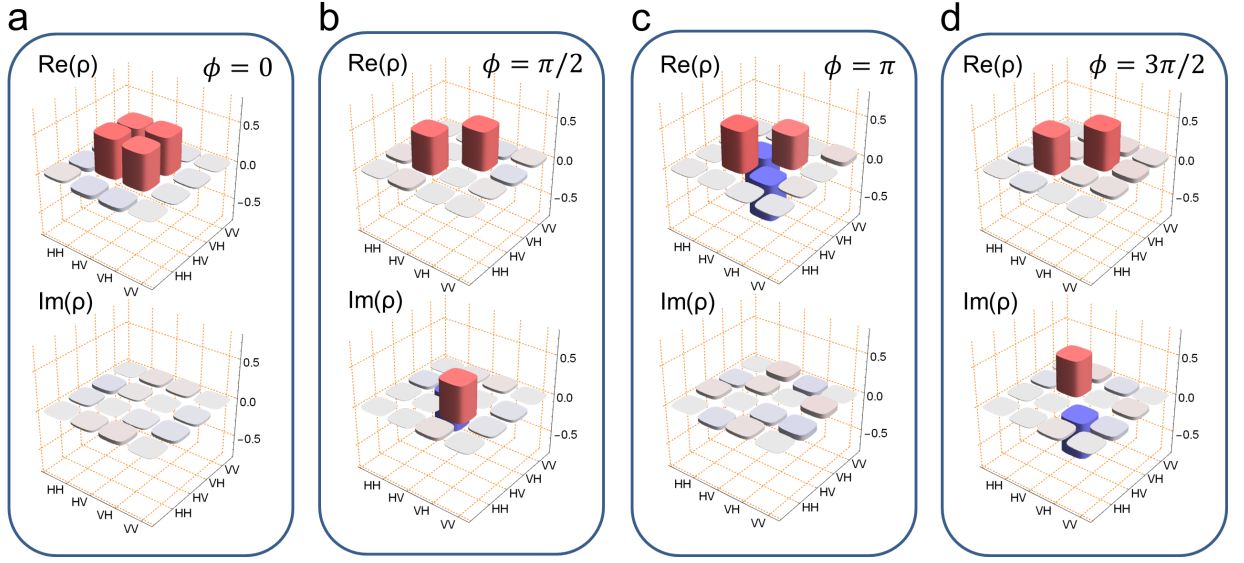


FIG. 10. Reconstructed density matrices of the output state after the entangled operation $\mathcal{O}_{AB} = 1/\sqrt{2}(\sigma_z \otimes \sigma_z + e^{i\phi} \sigma_x \otimes \sigma_x)$. Input state is prepared to $|HV\rangle$ and the expected output state after the entangled operation is $1/\sqrt{2}(|HV\rangle + e^{i\phi}|VH\rangle)$. The reconstructed density matrices of the output states correspond to (a) $\phi = 0$, (b) $\pi/2$, (c) π , and (d) $3\pi/2$. Note that the upper (lower) rows corresponds to the real (imaginary) part of the density matrices. The average fidelity between the ideal output state and the experimentally obtained output state is $F_{\text{ave}} = 0.933 \pm 0.010$ and the average concurrence of the output states $C = 0.904 \pm 0.018$. We performed Monte-Carlo simulations on reconstructing density matrices of each output state 100 times and calculated experimental errors. Here the errors on each quantity corresponds to one standard deviation.

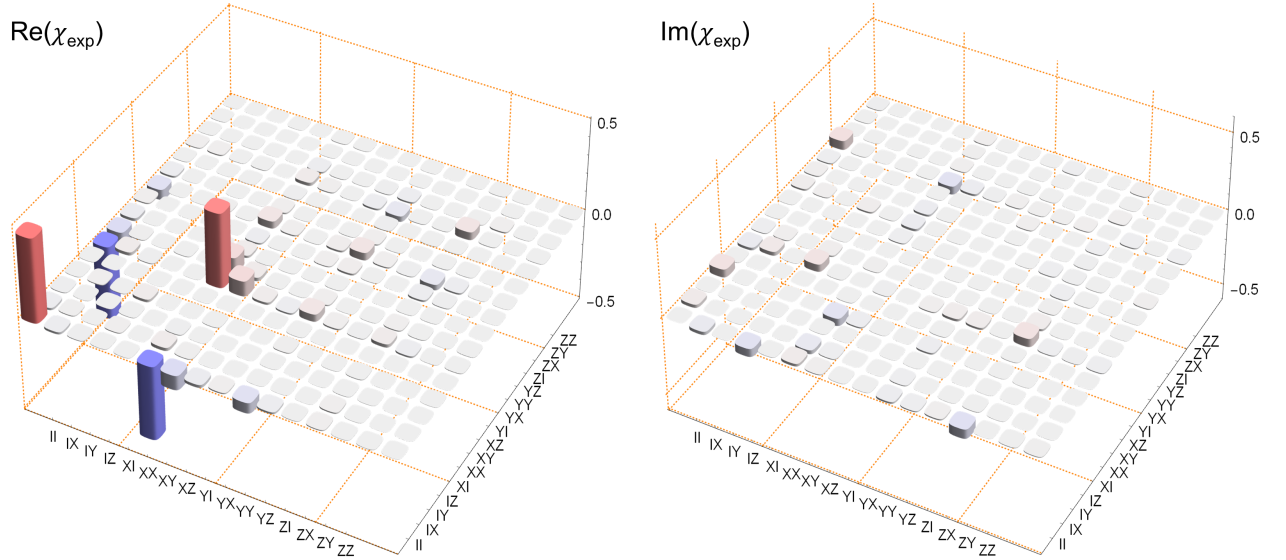


FIG. 11. Experimentally reconstructed process matrices χ of the entangled operation $\frac{1}{\sqrt{2}}(I \otimes I - \sigma_x \otimes \sigma_x)$. Left (right) columns corresponds to the real (imaginary) part of the process matrices. Process matrices are represented in the Pauli basis.

-
- [1] P. Zanardi, Entanglement of quantum evolutions, *Phys. Rev. A* **63**, 040304(R) (2001).
- [2] P. Zanardi, G. Vidal, and L. S. Faoro, Entangling power of quantum evolutions, *Phys. Rev. A* **62**, 030301(R) (2000).
- [3] W. Dür, G. Vidal, J. I. Cirac, N. Linden, and S. Popescu, Entanglement Capabilities of Nonlocal Hamiltonians, *Phys. Rev. Lett.* **86**, 544 (2001).
- [4] X. Wang and P. Zanardi, Quantum entanglement of unitary operators on bipartite systems, *Phys. Rev. A* **66**, 044303 (2002).
- [5] M. A. Nielsen, C. M. Dawson, J. L. Dodd, A. Gilchrist, D. Mortimer, T. J. Osborne, M. J. Bremner, A. W. Harrow, and A. Hines, Quantum dynamics as a physical resource, *Phys. Rev. A* **67**, 052301 (2003).
- [6] A. Zavatta, V. Parigi, M. S. Kim, H. Jeong, and M. Bellini, Experimental Demonstration of the Bosonic Comutation Relation via Superpositions of Quantum Operations on Thermal Light Fields, *Phys. Rev. Lett.* **103**, 140406 (2009).
- [7] X.-C. Yao, J. Fiurásek, H. Lu, W.-B. Gao, Y.-A. Chen, Z.-B. Chen, and J.-W. Pan, Experimental Realization of Programmable Quantum Gate Array for Directly Probing Commutation Relations of Pauli Operators, *Phys. Rev. Lett.* **105**, 120402 (2010).
- [8] Y.-S. Kim, H.-T. Lim, Y.-S. Ra, and Y.-H. Kim, Experimental verification of the commutation relation for Pauli spin operators using single-photon quantum interference, *Phys. Lett. A* **374**, 4393 (2010).
- [9] O. Oreshkov, F. Costa, and C. Brukner, Quantum correlations with no causal order, *Nat. Commun.* **3**, 1092 (2012).
- [10] G. Chiribella, G. M. D'Ariano, P. Perinotti, and B. Valiron, Quantum computations without definite causal structure, *Phys. Rev. A* **88**, 022318 (2013).
- [11] L. M. Procopio, A. Moqanaki, M. Araújo, F. Costa, I. A. Calafell, *et al.* Experimental superposition of orders of quantum gates, *Nat. Commun.* **6**, 7913 (2015).
- [12] P. A. Guérin, A. Feix, M. Araújo, and C. Brukner, Exponential Communication Complexity Advantage from Quantum Superposition of the Direction of Communication, *Phys. Rev. Lett.* **117**, 100502 (2016).
- [13] K. Wei, N. Tischler, S.-R. Zhao, Y.-H. Li, J. M. Arrazola, Y. Liu, *et al.* Experimental Quantum Switching for Exponentially Superior Quantum Communication Complexity, *Phys. Rev. Lett.* **122**, 120504 (2019).
- [14] G. Rubino, L. A. Rozema, A. Feix, M. Araújo, J. M. Zeuner, *et al.* Experimental verification of an indefinite causal order, *Sci. Adv.* **3**, e1602589 (2017).
- [15] K. Goswami, C. Giarmatzi, M. Kewming, F. Costa, C. Branciard, J. Romero, and A. G. White, Indefinite Causal Order in a Quantum Switch, *Phys. Rev. Lett.* **121**, 090503 (2018).
- [16] X. Zhao, Y. Yang, and G. Chiribella, Quantum metrology with indefinite casual order, Preprint available at arXiv:1912.02449 (2019).
- [17] Y. Guo, X.-M. Hu, Z.-B. Hou, H. Cao, J.-M. Cui, *et al.* Experimental Transmission of Quantum Information Using a Superposition of Causal Orders, *Phys. Rev. Lett.* **124**, 030502 (2020).
- [18] M. A. Nielsen, and I. L. Chuang, *Quantum Computation and Quantum Information* (Cambridge University Press, Cambridge, England, 2000).
- [19] E. Knill, R. Laflamme, and H. J. Milburn, A scheme for efficient quantum computation with linear optics, *Nature* **409**, 46 (2001).
- [20] S. Barz, Quantum computing with photons: introduction to the circuit model, the one-way quantum computer, and the fundamental principles of photonic experiments, *J. Phy. B: At. Mol. Opt. Phys.* **48**, 083001 (2015).
- [21] H. F. Hofmann and S. Takeuchi, Quantum Filter for Non-local Polarization Properties of Photonic Qubits, *Phys. Rev. Lett.* **88**, 147901 (2002).
- [22] R. Okamoto, J. L. O'Brien, H. F. Hofmann, T. Nagata, K. Sasaki, *et al.* An Entanglement Filter, *Science* **323**, 483 (2009).
- [23] X.-Q. Zhou, T. C. Ralph, P. Kalasuwan, M. Zhang, Peuzzo A. *et al.*, Adding control to arbitrary unknown quantum operations, *Nat. Commun.* **2**, 413 (2011).
- [24] Y. Lu, S. Zhang, K. Zhang, W. Chen, Y. Shen, *et al.* Global entangling gates on arbitrary ion qubits, *Nature* **572**, 363 (2019).
- [25] M. A. Nielsen and I. L. Chuang, Programmable quantum gate arrays, *Phys. Rev. Lett.* **79**, 321(1997).
- [26] L. Slodicka, M. Jezek, and J. Fiurásek, Experimental demonstration of a teleportation-based programmable quantum gate, *Phys. Rev. A*, **79**, 050304 (2009).
- [27] T. F. Watson, S. G. Philips, E. Kawakami, D. R. Ward, P. Scarlino, *et al.* A programmable two-qubit quantum processor in silicon, *Nature* **555**, 633 (2018).
- [28] J. D. Franson, Two-photon interferometry over large distances, *Phys. Rev. A* **44**, 4552 (1991).
- [29] R. T. Thew, A. Acin, H. Zbinden, and N. Gisin, Bell-Type Test of Energy-Time Entangled Qutrits, *Phys. Rev. Lett.* **93**, 010503 (2004).
- [30] D. F. V. James, P. G. Kwiat, W. J. Munro, and A. G. White, Measurement of qubits, *Phys. Rev. A* **64**, 052312 (2001).
- [31] J. Fiurásek and Z. Hradil, Maximum-likelihood estimation of quantum processes, *Phys. Rev. A* **63**, 020101 (2001).
- [32] J. A. Jones, Robust Ising gates for practical quantum computation, *Phys. Rev. A* **67**, 012317 (2003).
- [33] S. Debnath, N. M. Linke, C. Figgatt, K. A. Landsman, K. Wright, *et al.* Demonstration of a small programmable quantum computer with atomic qubits, *Nature* **536**, 63 (2016).
- [34] B. Kraus and J. I. Cirac, Optimal creation of entanglement using a two-qubit gate, *Phys. Rev. A* **63**, 062309 (2003).
- [35] M. W. Coffey and R. Deiotte, Relation of operator Schmidt decomposition and CNOT complexity, *Quant. Info. Process.* **7**, 117 (2008).
- [36] S. Agne, T. Kauten, J. Jin, E. Meyer-Scott, J. Z. Salvail, D. R. Hamel, K. J. Resch, G. Weihs, and T. Jennewein, Observation of Genuine Three-Photon Interference, *Phys. Rev. Lett.* **118**, 153602 (2017).
- [37] D. M. Greenberger, M. A. Horne, and A. Zeilinger, Going beyond Bell's theorem. In *Bell's theorem, quantum theory and conceptions of the universe* (1989) (pp. 69-72). Springer, Dordrecht.
- [38] W. Dür, G. Vidal, and J. I. Cirac, Three qubits can be entangled in two inequivalent ways, *Phys. Rev. A* **62**, 062314 (2000).
- [39] B. P. Lanyon, M. Barbieri, M. P. Almeida, T. Jen-

- newein, T. C. Ralph, *et al.* Simplifying quantum logic using higher-dimensional Hilbert spaces, *Nat. Phys.* **5**, 134 (2009).
- [40] V. Alba, J. Dubail, and M. Medenjak, Operator Entanglement in Interacting Integrable Quantum Systems: The Case of the Rule 54 Chain, *Phys. Rev. Lett.* **122**, 250603 (2019).
- [41] M. Araujo, A. Feix, F. Costa, and C. Brukner, Quantum circuits cannot control unknown operations, *New J. Phys.* **16**, 093026 (2014).
- [42] M. Araujo, F. Costa, and C. Brukner, Computational Advantage from Quantum-Controlled Ordering of Gates, *Phys. Rev. Lett.* **113**, 250402 (2014).
- [43] Y. Cao, J. Romero, J. P. Olson, M. Degroote, P. D. Johnson, *et al.* Quantum computations without definite causal structure, *Chem. Rev.* **119**, 10856 (2019).
- [44] F. Klauck, L. Teuber, M. Ornigotti, M. Heinrich, S. Scheel, *et al.* Observation of PT-symmetric quantum interference, *Nat. Photon.* **13**, 883 (2019).
- [45] H.-T. Lim, Y.-S. Ra, K.-H. Hong, S.-W. Lee, and Y.-H. Kim, Fundamental Bounds in Measurements for Estimating Quantum States, *Phys. Rev. Lett.* **113**, 020504 (2014).
- [46] J. Brendel, W. Dultz, and W. Martienssen, Geometric phases in two-photon interference experiments, *Phys. Rev. A* **52**, 2551 (1995).
- [47] K. Sanaka, K. Kawahara, and T. Kuga, New High-Efficiency Source of Photon Pairs for Engineering Quantum Entanglement, *Phys. Rev. Lett.* **86**, 5620 (2001).
- [48] A. Rossi, G. Vallone, F. De Martini, and P. Mataloni, Generation of time-bin-entangled photons without temporal postselection, *Phys. Rev. A* **78**, 012345 (2008).